High frequency tide-surge-river interaction in estuaries: causes and implications for coastal flooding

Preston Spicer[1], Kimberly Huguenard[1], Lauren Ross[1], and Laura N. Rickard[2]

[1]Department of Civil and Environmental Engineering, University of Maine, Orono, ME, USA.
[2]Department of Communication and Journalism, University of Maine, Orono, ME, USA.

Corresponding author: P. Spicer (preston.spicer@maine.edu)

Key Points:

- Tide-surge-river interaction was shown to be largest in the 6^{th} and 8^{th} diurnal bands.
- High frequency tide-surge-river interaction can have amplitudes more than double that of low frequency surge.
- Enhanced bottom friction and resonance were the primary mechanisms causing tide-surge-river interaction at the D_6 and D_8 bands.

Abstract

Tide-surge interaction creates perturbations to storm surge at tidal frequencies and can affect the timing and magnitude of surge in tidally energetic regions. To date, limited research has identified high frequency tide-surge interaction (> 4 cycles per day) in coastal areas, and its significance in fluvial estuaries (where we consider it tide-surge-river interaction) is not well documented. Water level and current velocity observations were used to analyze tide-surge-river interaction at multiple tidal and overtide frequencies inside of a shallow estuary. Near the head of the estuary, higher frequency harmonics dominate tide-surge-river interaction and produce amplitudes more than double that of wind and pressure-driven surge. Bottom friction enhanced by storm-induced currents is the primary mechanism behind the interaction, which is further amplified by within-estuary resonance. High frequency tide-surge-river interactions in estuaries present a significant threat to human life, as the onset of flooding (in < 1.5 hrs.) is more rapid than coastal storm surge flooding. Commonly used storm surge forecasting models neglect high frequency tide-surge-river interaction and thus can markedly underestimate the magnitude and timing of inland storm surge flooding.

Plain Language Summary

Storm surges are a threat to life and property on the coast. How storm surges interact with tides varies by region and is not well understood, particularly in estuaries. This tide-surge interaction, which we identify as tide-surge-river interaction in estuaries with a strong river influence, can affect the timing and magnitude of storm surges, and so is important to understand. This study calculated storm surge and tide-surge-river interaction in a large estuary with strong tides after collecting water levels in the system for one Fall / Winter season. Results show that tide-surge-

river interaction can more than double storm surges relative to the non-tide influenced surge and create rapid oscillations to water level that are hard to predict. Enhanced current velocities during storms from wind and surge propagation can cause tide-surge-river interaction, which can be further amplified by estuary geometry. Common surge models do not accurately resolve these high frequency tide-surge-river interactions.

1 Introduction

Storm surges present a risk to life and property in coastal communities (von Storch & Woth, 2008). Recent studies predict that climate change can regionally increase storminess, storm surge heights (Lowe & Gregory, 2005), and tidal ranges (Devlin et al., 2017; Holleman & Stacey, 2014), collectively enhancing the threat of flooding from storm surge. Furthermore, nonlinear components of the tide are expected to increase with sea level rise (Holleman & Stacey, 2014), thereby enhancing the complexity of coastal flood forecasting. The socioeconomic loss associated with coastal flooding can be substantial (e.g., 80,000 businesses negatively affected by Hurricane Katrina in 2005) (Petterson et al., 2006), demonstrating the need to advance the current understanding of storm surge behavior to mitigate damage on the coast.

Storm surge is quantified as the difference between the predicted tide and the observed water level during a storm event. Low-frequency surge is the component to surge which modifies the non-tidal water level (water level assuming no tidal influence) during storm events and includes contributions from wind set-up, atmospheric pressure, and river discharge (Pond & Pickard, 1983). Low frequency surge can be externally generated in the coastal ocean and propagate into

an estuary, or internally generated within the estuary. Tide-surge interaction, which is how the tide interacts with the low frequency surge, manifests as an oscillation to surge at tidal frequencies, and can be created one of two ways: (1) the tide can modify an externally generated surge; and/or (2) a locally generated surge can modify the tide, with each case dependent on how surge propagates relative to the tide (Horsburgh & Wilson, 2007; Rossiter, 1961). Many coastal flood and storm surge models consider only low-frequency surge for simplicity (e.g. Fanjul et al., 2001; Glahn et al., 2009) which neglects more computationally expensive and complicated nonlinear tide-surge interactions. This straightforward approach may sacrifice accuracy, as some studies have reported root mean square errors of observed water levels at 70% of predicted water levels (Qin et al., 1994). Fig. 1 illustrates how tide-surge interaction can enhance coastal flooding by increasing the total water level above the contribution of wind and pressure-driven surge. Tide-surge interaction has been identified at varying levels of significance in localized regions, generally on the coast.

Recent storm surge studies emphasize the development of tide-surge interaction over the shelf regions on the coast. Atmospheric pressure (Mercer, 2002) and wind (Rego & Li, 2010; Feng et al., 2016) often play an important role in the creation of the interaction, but other factors like steepness of the continental shelf and wave set-up (Nayak et al., 2012) can also contribute. Nonlinear bottom friction is often considered the dominant mechanism causing the interactions (Rego & Li, 2010; Feng et al., 2016; Wolf, 1978; Valle-Levinson et al., 2013; Jones & Davies, 2008), but tide-surge interaction can also be influenced by shallow water and advection (Rego & Li, 2010; Wolf, 1978; Wolf, 1981). Observed tide-surge interaction on the coast has reached magnitudes of up to 80% of principal tidal amplitudes (Rego & Li, 2010), but tide-surge interaction is not usually larger than the contribution from low-frequency surge. However, recent

95 studies have shown that tide-surge interaction in estuaries produces larger amplitudes than those
96 found on the immediate coast (Horsburgh & Wilson, 2007; Thomas et al., 2019).

97 Estuaries often feature complex characteristics that can modify the tidal signal and may
98 cause tide-surge interaction to behave differently than the coast (Lyddon et al., 2018). Pioneering
99 work in the 1950s used a 1-dimensional analytical model to understand how the principal tide
100 and an externally generated storm surge interact in a simple basin (Proudman, 1955a, 1955b)
101 suggesting that larger water levels from the presence of surge allowed for faster tidal propagation
102 and vice versa. The model compared well with observations near the mouth of the Thames River,
103 but discrepancies were evident upstream. Since then, many studies have used numerical models
104 (e.g. Rossiter, 1961; Prandle & Wolf, 1978; Horsburgh & Wilson, 2007; Thomas et al., 2019) to
105 examine the tide-surge interaction in more complex systems, though they focus on modification
106 to/from the principal tide. Higher frequency tides (overtides) can be influential in frictional and
107 fluvial estuaries and arise through indirect interactions between the principal tide and shallow
108 water, between harmonics, and between river discharge and harmonics (Parker, 1991). Higher
109 frequency tide-surge interactions (4th diurnal and larger) are not captured in the previously
110 mentioned model frameworks and have only been identified observationally (Horsburgh &
111 Wilson, 2007; Prandle & Wolf, 1978). The importance of these high frequency interactions in
112 estuaries has been largely ignored, as have the mechanisms that create them. Considering the
113 importance of both geometry and river discharge in creating nonlinear tidal interactions, the
114 authors will refer to high frequency storm surge in fluvial estuaries as tide-surge-river
115 interaction. The susceptibility of inland estuarine communities to storm surge flooding,
116 particularly through higher frequency tide-surge-river interaction, therefore remains to be
117 understood.

118 In following, the present study will: (1) determine the spatiotemporal variability of higher
119 frequency tide-surge-river interactions in estuaries; (2) assess the relative contributions of higher
120 frequency tide-surge-river interaction to overall surge levels; and (3) investigate the mechanisms
121 creating higher frequency tide-surge-river interactions. This research is the first work to identify
122 tide-surge-river interaction from enhanced storm-induced currents and resonance.

123

124 **2 Materials and Methods**

125 **2.1 Study Site**

126 Data for this research were collected in the Penobscot River estuary located on the central
127 coast of Maine in the United States (Fig.2). The Penobscot estuary, comprised of bay and river
128 sections, is a long, converging, and deep estuary extending approximately 100 km from the
129 Atlantic Ocean near Rockland to the head at Eddington, 6 km north of Bangor. The width of the
130 estuary varies from nearly 30 km in the lower bay to 0.24 km at Bangor. Maximum average
131 depths range from 120 m near the mouth to 30 m at the confluence with the river (boxed area in
132 Fig. 2b). Average depths in the riverine portion of the system then decrease to 5.5 m at Bangor.
133 The primary sources of freshwater are the Penobscot River and Kenduskeag Stream at Bangor.
134 The mean annual discharge at the confluence of these rivers is 396 m^3/s and the 100-year peak
135 flood is 3370 m^3/s (Hodgkins, 1999). High runoff periods generally occur during the spring
136 freshet (April to May) with a mean monthly discharge of 1105 m^3/s, while the lowest runoff
137 period is typically September with a mean monthly discharge of 140 m^3/s (Dudley, 2004). The
138 tidal range in the estuary ranges from about 2.9 m during neap tides to 4.9 m during spring tides
139 and tidal velocity amplitudes range from 0.7 m/s on neap tides to 1.3 m/s on springs (Geyer &

Ralston, 2018). Most major coastal storms in the region occur in the winter, usually as "Nor' Easters", characterized by strong winds blowing from the northeast.

2.2 Data Collection and Processing

2.2.1 Water Level and Currents

Three HOBO water level loggers were deployed in Penobscot Bay for part of the Fall and Winter of 2017/2018 (October 1st through January 31st) to measure water levels at Rockport (44.1855 N, 69.0737 W), Belfast (not shown) (44.4291 N, 69.0030 W), and Castine (44.38625 N, 68.79652 W) (Fig. 2b). Each sensor sampled at 2-minute intervals and featured a 0.1% measurement accuracy. The sensors measured absolute pressure, which was converted to water level using barometric pressure data. Water level measurements from a USGS river gage (Station #01037050 at 44.7961 N, 68.7679 W) in Bangor sampling at 6-minute intervals were also used to supplement these data. These water level data were part of the Sensing Storm Surge citizen science project initiated by an interdisciplinary team of University of Maine researchers (http://sensingstormsurge.acg.maine.edu/), with the Rockport, Belfast, and Castine sensors monitored by trained local volunteers. The most compelling data collected during the study period occurred during one storm event, which is explained further in Section 3. The Belfast sensor was not deployed during the time of that event, and so data from Belfast was not usable in this paper.

Current velocities were measured at 20-minute intervals at a depth of 2 m with an Aanderaa current meter from a buoy in eastern Penobscot Bay near Castine (44.3775 N, 68.8296

160 W). North-south (N-S) and east-west (E-W) components were recorded, with the N-S taken as
161 the along-channel component given the north-south orientation of the Penobscot estuary.

162 **2.2.2 Environmental Conditions**

163 Barometric pressure and wind data were collected in Castine and Bangor (Fig. 2b). The
164 Maine Maritime Academy weather station at Castine is approximately 45 km from Bangor and
165 30 km from Rockport on the eastern side of Penobscot Bay. Wind and barometric pressure were
166 sampled at 1-minute intervals at this location, with the barometric pressure used to calculate
167 water levels at Rockport and Castine. Wind was also recorded at Bangor International Airport,
168 approximately 5 km from the Bangor tide gauge, in 4-minute intervals. All wind data were
169 converted to oceanographic convention. River discharge was measured once daily at a USGS
170 river gauge (Station #01034500) on the Penobscot River in West Enfield, approximately 54 km
171 upstream of Bangor.

172 **2.3 Harmonic Analysis and Surge Decomposition**

173 The results of this study focus on one storm event, the October 30th, 2017 Windstorm.
174 This event featured a storm path and wind field that created the largest amplitude tide-surge-river
175 interaction over the monitoring period. Water level data were analyzed in a two-month period
176 covering October to November. Significant ice cover on the river in Bangor during December
177 and January created inconsistencies in water level data, and so that period was not used in
178 harmonic analysis. Data at Rockport and Castine were collected in monthly segments, thus

segments were concatenated and interpolated onto a uniform grid to create a continuous two-month time series.

A harmonic analysis and data filtering process following Feng et al. (2016) was conducted to extract components of surge from water level measurements. Water levels in the two-month segments at each location were demeaned and spikes were removed and interpolated with surrounding data. Predicted tides were then computed using the *T_Tide* MATLAB toolbox (Pawlowicz et al., 2002). At each station, the total surge (*TS*) was computed by subtracting the predicted tide (*PT*) from the demeaned observed total water levels (*TWL*). The total surge is comprised of a tidal component and non-tidal component. The non-tidal surge, called low frequency surge (*LFS*) was extracted from the residual using a Fourier low-pass filter with a cut-off period of 30 hours (Walters & Heston, 1982), thus excluding all tidal frequencies that are diurnal and higher. An average form factor ($F = \frac{K_1+O_1}{M_2+S_2}$) of 0.11 in the estuary shows the tides are mixed, mainly semidiurnal, justifying this cut-off period. Low-frequency surge represents the demeaned non-tidal water level and includes influences from river discharge, as well as wind and pressure-driven storm surge. The tide-surge-river interaction term (*I*), was calculated by subtracting *LFS* from *TS*. The interaction term physically represents either how the tide changes an externally generated, propagating wave (i.e. storm surge) or how water level residuals modify the tides. Fig. 3, scaled with the actual results of the October Windstorm in Bangor (elaborated on in Section 3), conceptually shows these components to *TWL* relative to mean sea level and how the summation of *PT*, *LFS* and *I* can produce water levels larger than *PT*+*LFS* when nonlinear surge (*I*) amplifies. The harmonic analysis was also applied to the current velocities to

distinguish tidal current velocities from non-tidal current velocities influenced by other mechanisms, such as wind, storm surge and river discharge.

2.4 Wavelet Transforms and Reconstruction of Tides and Tide-Surge-River Interaction

To understand the mechanisms creating tide-surge-river interaction, the specific tidal and overtide frequencies in *I* need to be identified. To do so, a wavelet analysis (Torrence & Compo, 1998) was performed on each time series of *I*. Wavelets were also created for *PT* at each location to highlight how the tide-surge-river interaction manifested in water levels. The wavelet transform is used in this study as a tool to analyze time series that contain non-constant power to see how harmonics, or harmonic ranges (bands), within the series change with time. From the wavelets (*PT* and *I*), signals were re-created at the D_2, D_4, D_6, and D_8 bands to identify exact variations in amplitude and phase of each band around storm events. All data at each location were interpolated onto grids with a 15 second time interval prior to wavelet analysis to ensure equal comparison. The time interval chosen provided filter lengths and bands small enough to capture the dominant harmonics of interest within each band, without losing time resolution (Kukulka & Jay, 2003). The D_2 band includes all signals with periods between 11 and 14.5 hours, the D_4 covers 5.5 to 7 hours, the D_6 covers 4 to 4.5 hours, and the D_8 includes 2.7 to 3.2 hours. Bands, rather than specific harmonics, were resolved because the signal reconstruction analysis described next does not always allow for specific harmonics to be re-created.

Following Torrence & Compo (1998), the base wavelet function, $\psi_0(\eta)$, should be chosen based on the data set being analyzed. In this analysis, a Morlet base function is used; a nonorthogonal, complex function. Nonorthogonal transforms are best for time series where smooth and continuous variations in wavelet amplitude are expected, while complex functions

return information on both amplitude and phase, allowing for better depictions of oscillatory behavior in the time series. Given the base function, a continuous wavelet transform at each scale, *s*, is calculated as:

$$W_n(s) = \sum_{k=0}^{N-1} \hat{x}_k \hat{\psi} * (s\omega_k) e^{i\omega_k n \delta t} \quad (1)$$

where k = 0…*N*-1 is the frequency index with *N* being the number of points in the series, $\hat{x}_k$ is the discrete Fourier transform of the time series, $\hat{\psi} * (s\omega_k)$ is the complex Fourier transform of the wavelet function, $\omega_k$is the angular frequency, *i* is the scale index, *n* is the localized time index, and δt is the equal time spacing which the transform follows. Calculating $W_n(s)$ at each scale then allows for the tidal and overtide signals in both *PT* and *I* to be reconstructed, as the sum of the real part of the wavelet transform over the scales of each frequency:

$$x_n = \frac{\delta i \delta t^{\frac{1}{2}}}{C_\delta \psi_0(0)} \sum_{i=0}^{I} \frac{\Re\{W_n(s_i)\}}{s_i^{1/2}} \quad (2)$$

where C_δ is the unitless reconstruction factor, taken as 0.776 and $\psi_0(0)$ is the unitless energy scaling factor, taken as $\pi^{-1/4}$, both of which are constant for a Morlet base (Torrence & Compo, 1998). δi determines the resolution of scales and is taken as 0.25, δt is the sampling interval of the time series, *i* and *I* are the lower and upper scale indices, respectively, of the band being reconstructed, $\Re\{W_n(s_i)\}$ is the real part of the wavelet transform at each scale, and s_i is the scale itself:

$$s_i = s_0 2^{i\delta i}, \quad i=0, 1, \ldots, I \quad (3)$$

The reconstruction analysis elucidates how various components to the tide and surge change with time, which can be compared with environmental conditions to identify the forcing mechanisms

242 contributing to each harmonic. This harmonic analysis, decomposition, and reconstruction
243 analysis was repeated on along-channel (north-south) currents to investigate how quadratic
244 friction ($\frac{C_D u|u|}{h_0}$) was modified during each event.

245

246 **3 Results**

247 **3.1 October 30th "Windstorm"**

248 The October 30st, 2017 storm, locally referred to as the "October Windstorm", was a
249 hybrid storm created from the remnants of a tropical storm over the southeast United States
250 merging with a low-pressure system moving over the Great Lakes. This storm was a bomb
251 cyclone, identified by a drop of over 24 mb in barometric pressure at the center in 24 hours,
252 producing rapid intensification. The center of the storm passed to the west of Maine from New
253 York City into Canada (Fig. 4). Penobscot Bay was located on the eastern side of the storm,
254 which promoted onshore 20 m/s sustained winds and a barometric pressure minimum of 982 mb.
255 River discharge was elevated (~750 m^3/s) during the October Windstorm, compared to the mean
256 annual discharge of 396 m^3/s. Results show storms of this size and characteristics can produce
257 significant high-frequency tide-surge-river interaction, and so provided an opportunity to study
258 the phenomenon and how it evolves along an estuary. The ramifications of events such as this on

estuarine flooding is important, particularly during the fall / winter seasons when windstorms are known to impact the region.

3.2 Tide-Surge-River Interaction

The October Windstorm featured *LFS* over 1.5 days in the Penobscot River (day 29.6 to 31.1 in Fig. 5a [1,2,3]). The *LFS* exhibited properties of an externally generated solitary wave, evidenced by an amplification between peak values at Rockport (0.35 m) to Castine (0.49 m), then Bangor (0.71 m); phase lag of 2.1 hours between the mouth (Rockport) and head (Bangor); and a crest to no-trough profile indicative of solitary waves (Fig. 5a [1,3]). The funnel-like shape of the estuary likely influenced the amplification, enhancing the externally generated surge in a similar manner to the tides (Friedrichs, 2010). At all locations, maximum values of *LFS* occurred at or just after high water at the beginning of the ebb tide (Fig. 5b [1,2,3]). Tide-surge-river interaction was identified in D_2, D_4, D_6, and D_8 bands during the storm. The interaction increased both upstream and with each higher order harmonic (excluding Rockport) (Fig. 5).

At the head of the estuary in Bangor, the tide-surge-river interaction contributed to a total surge (2 m) that was almost three times larger than *LFS* alone (Fig. 5a [1]). The amplitude of the D_2 component of *I* began increasing at the start of the *LFS*, peaked on the ebb tide following the maximum *LFS* (0.25 m at day 30.5 in Fig. 5b [1]), and was phase shifted by 0.2 hrs. relative to the mouth. The amplitude of the D_4 interaction peaked at day 30.4 (0.38 m), which was nearly double that of the predicted D_4 tide (0.17 m) (Fig. 5b [1]). Both the D_6 and D_8 *I* began amplifying around day 30.3 at slack water and were maintained until days 31 and 31.3, respectively (Fig. 5d [1], e [1]). The maximum amplitude of the D_6 band of *I* (0.73 m) occurred at day 30.6 on slack tide, as did the D_8 (0.96 m), both of which were significantly larger than the predicted tidal

amplitudes at the time (0.05 m and 0.04 m, respectively, in Fig. 5d [1], e [1]). With *LFS* near 0.7 m, the D_6 and D_8 bands together produced ~1.7 m of surge, making them the most significant contributors to *I*, and subsequently *TS*.

In Rockport at the mouth of the estuary, tide-surge-river interaction was evident but much less pronounced. Total surge levels were 0.8 m, which were more than double *LFS* alone (Fig. 5a [3]). At this location, amplitudes of *I* in the D_2, D_4, D_6, and D_8 bands peaked at 0.11 m, 0.17 m, 0.16 m, and 0.15 m, respectively during the storm (Fig. 5b [3], c [3], d [3], e [3]), and showed the contribution from D_4 surpassed that of D_6 and D_8. The amplification upstream was smallest in the D_4 band (2.4 times larger at the head of the estuary than the mouth) relative to D_6 and D_8 (5 and 6 times larger, respectively). Amplitudes of *I* in the D_6 and D_8 bands peaked earlier in Rockport (ebb tide at day 30.4 in Fig. 5d [3], e [3]) than in Bangor (slack tide at day 30.6 in Fig. 4d [1], e [1]), another indication that the surge was externally generated and propagated into the estuary.

Tide-surge-river interaction and total surge amplitudes in Castine generally fell between those observed at Rockport and Bangor. Total surge peaked at 1 m, which, like the other locations, was approximately double that of *LFS* (Fig. 5a [2]). Amplitudes of *I* in the D_2, D_4, D_6, and D_8 peaked at 0.07 m, 0.18 m, 0.27 m, and 0.36 m, respectively (Fig. 4b [2], c [2], d [2], e [2]), showing Castine is near the point along-estuary where the D_6 and D_8 surpass the amplitude of D_4 tide-surge-river interaction. Peak interaction in both the D_6 and D_8 occur slightly after the corresponding peaks in Rockport (day 30.4-30.5 in Fig. 5d [2], e [2]), but before Bangor.

These results showed that high-frequency harmonics (D_4, D_6, and D_8) that contribute to tide-surge-river interaction more than doubled total surge levels in the Penobscot River. The

largest contributions (from the D_6 and D_8 bands) are tied to quadratic friction, $\frac{C_D u|u|}{h_0}$ (where C_D is the drag coefficient, u is the current velocity, and h_0 is average depth). The D_8 band is formed from the interaction of the D_6 and D_2 bands and quadratic friction is the only mechanism driving sixth-diurnal oscillations if the M_2 harmonic is the principal tide (Parker, 1991).

3.3 Frictional mechanism

During the October Windstorm, non-tidal currents were likely influenced by wind, storm surge, density-induced flow, and river discharge. The non-tidal flow featured maximum landward velocity of ~0.37 m/s just prior to the maximum *LFS* (day 30.3 in Fig. 6a, b), after which it reversed direction to a maximum seaward velocity of -0.33 m/s (day 30.9 in Fig. 6a, b). When storm surge propagates as a solitary wave in the presence of an opposing current (i.e., river discharge), the velocity field under the wave tends to be upward on the foreside of the crest, horizontal in the direction of wave propagation under the crest of the wave and directed downward on the aft side of the crest (Zhang et al., 2015). Based on conditions occurring at the time, it is possible the landward velocity under the *LFS* crest combined with currents driven by a strong onshore wind (10 m/s N-S and -8.7 m/s E-W in Fig. 6a) overcame seaward directed river discharge and density-driven flows. On the aft side of the crest, density-driven flow and river discharge presumably combined to create the seaward non-tidal current peak of similar magnitude to the prior landward flow. To investigate if the non-tidal flows could enhance the higher frequency tide surge interactions, the quadratic friction was quantified. Assuming a C_D of 0.003 (Geyer, 1993) and h_0 of 25 m (depth at Castine buoy), the quadratic friction terms were calculated for both the *PT* and *I* at the D_2 band (Fig. 6c). The amplitude of the quadratic friction from the interaction term increased from 0 to about 0.5 m/s^2 during peak landward and seaward

non-tidal currents (days 30 to 31.2 in Fig. 6). Quadratic friction from *PT* was in phase with quadratic friction from *I* during that time, during which *I* increased both in water level and currents (Fig. 6c, d).

4 Discussion

During the observed storm event, high frequency tide-surge-river interaction amplified upstream and more than doubled total surge levels. Contributions from sixth and eighth diurnal oscillations in storm surge accounted for the majority of the tide-surge-river interaction that enhanced overall surge. To understand why the D_6 and D_8 oscillations of tide-surge-river interaction were enhanced during storm events, the physical mechanisms that contribute to each must be determined. Tide-surge-river interaction in the principal D_2 band is required for the overtide frequencies to be present, and so is first discussed.

4.1 D_2 and D_4 Tide-Surge-River Interaction

Tide-surge-river interaction in the D_2 band at each location featured a positive interaction on each ebb tide and a negative on flood (Fig. 5b [1]), indicating that the tidal wave amplitude is augmented during ebb tide and opposed during flood tide. Previous tide-surge-river interaction studies observe storm surge peaks during flood tide because *PT*+*I* precede *PT* as the shallow water wave speed increases in deeper water (e.g. Horsburgh & Wilson, 2007; Rossiter, 1961; Proudman, 1955a, 1955b), however the phase shift in the tide can also be produced by river discharge (Parker, 1991). The October Windstorm occurred near the maximum river discharge during the study period, making this a likely explanation for the phase shift in the principal tide

amplitude. Using the shallow water wave speed equation (with mean flow): $\boldsymbol{c = U_0 + \sqrt{gh}}$, where c is the wave speed, U_0 is a depth-uniform mean current, g is the gravitational constant, and h is a mean depth (Dean & Dalrymple, 1991); the effect of mean river flow on the tide can be estimated. Using the estuary mean depth of 15 m, a shallow water wave propagating against a 0.75 m/s river current (estimate from river discharge and average river cross sectional area) would arrive in Bangor 0.2 h later than one without a mean flow, matching the observed phase difference between *P* and *PT+I* (not shown). Furthermore, *LFS* surge peaks in Bangor 2.1 h after Rockport for this storm event, matching the expected travel time of a solitary wave (Zhang et al., 2015) and providing justification for the slower rise to *LFS* peak than the fall. A simple correlation between river discharge and the phase difference between the D_2 amplitude of *PT* and *PT+I* was determined for a 20-day period surrounding the storm (October 20th to November 9th). The correlation produced a coefficient of 0.74 with 95% CI of [0.59, 0.82], indicating that the D_2 interaction was indeed a result of a mean flow interacting with the principal tide. However, the contribution of the principal tidal harmonic (D_2) to tide-surge-river interaction was small relative to the contributions from higher frequency (overtide) bands.

The D_4 component to *I* is larger than the D_2, but the D_6 and D_8 bands independently augment *I* more than the D_4. The D_6 interaction term is largest when peak non-tidal current velocities enhance quadratic friction on both phases of the tide, indicating that storm-induced currents can have a significant effect on overtide amplitudes. Initial amplification of *I* in the D_6 and quadratic friction from *I* in the D_2 aligned with the landward non-tidal flow (Fig. 6); when a flood tide, northward winds, and externally generated *LFS* collectively contributed to a net landward flow (Fig. 7a, quantified using a simple 1-D momentum balance [Geyer, 1993]). The amplified quadratic friction and D_6 oscillation continued until after day 30.9, when an ebb tide,

decreasing *LFS*, density driven flow, and large river flow (relative to average), created a net seaward flow (Fig. 6, 7b). Therefore, storm induced non-tidal currents enhanced the quadratic friction creating the amplified D_6 oscillation, which maintained until non-tidal currents decreased back to magnitudes near zero. This is corroborated by a 0.86 correlation coefficient (with 95% CI of [0.82, 0.88]) between 5 days (day 28 to 33) of north-south non-tidal flow and the D_6 interaction. It is very likely that enhancement of the D_6 would not have been as notable if the *LFS* from this storm did not propagate into the estuary and contribute to non-tidal flows and was rather generated inside the estuary. The majority of more traditional "Nor'easter" storms occurring in the winter of 2017-2018 passed along the coast and created internally generated surge without significant D_6 oscillations (not shown).

4.2 Quadratic Friction and Resonance Enhancing D_6 and D_8 Tide-Surge-River Interaction

The D_8 band of *PT+I* should only surpass the D_6 if near resonance with the estuary, according to general compound tide theory (Parker, 1991). Results show this happens during the October Windstorm (day 30.6 thru 30.8 in Fig. 4), indicating the D_8 band is near the natural frequency of the Penobscot estuary. When a harmonic is resonant, incident waves at that frequency moving into an estuary are constructively reinforced by reflected waves moving out, amplifying the harmonic. Generally, reflected waves in convergent estuaries dissipate quickly as they move seaward due to divergence and friction reducing wave energy. The Penobscot estuary is convergent in shape (mainly in the bay), allowing for the tidal amplitude to increase (~0.5 m, not shown) from mouth to head (convergence dominates friction). However, far upstream, where the tidal amplitudes are largest, the estuary is relatively uniform in width (Fig. 2b), creating

conditions where a reflected wave could be maintained before re-entering the bay. A simple formula can be used to determine resonant period given a depth and wavelength in a system:

$$\boldsymbol{T = \frac{4L}{\sqrt{gh}}} \qquad (4)$$

where T is the resonant period, L is the estuary length, g is the gravitational acceleration, and h is the mean depth of the estuary. Equation (4) outlines that resonance will occur when the natural period of the estuary is the same as a tidal or overtide period. The D_8 *PT*+*I* amplitude exceeds D_6 in Bangor and Castine (upstream in the width-uniform portion of the estuary), indicating that resonance is likely constrained to the shallower reaches of the Penobscot estuary (Fig. 2). The length, L, used in Equation (4) is taken as the river length from Bangor to the entrance of the bay, shown as the boxed area in Fig. 2b, where depths vary between 15 m and 5 m. With L = 28,000 m, and the average period of the D_8 band, T = 3 h, the resonant depth, h, was calculated as 11 m, which is deeper than the average depth calculated over the river section (8.5 m). Based on this calculation, an increase in mean water level from *LF*S would bring the estuary closer to resonance.

There are five instances over the study period (between October and January) when the D_8 *PT*+*I* is larger than the D_6, and four occur when there is an increase in average depth from *LFS* that coincides with an increase in the D_6 component of *I*. Furthermore, the October Windstorm created the largest of both *LFS* and D_8 *PT*+*I* amplitudes, respectively, over the study period. The onset of enhanced D_8 oscillations can cause water levels to abruptly rise (within approximately one-half of the period of the D_8 component [1.5 hrs.]) compared to typical *LFS* (Fig. 5a [1]), presenting potentially hazardous conditions to life and property. A significant

account from Bangor in the 1970s presents evidence of these rapid, dangerous oscillations to storm surge.

4.3 Historical Support

On February 2, 1976, a coastal storm flooded downtown Bangor after producing a 3.2 m storm surge (Morrill et al., 1979). The storm passed over western Maine following a similar track to the October Windstorm (Fig. 4a). A central pressure of 964 mb was recorded in western Maine and maximum sustained winds of 21 m/s toward the northwest were recorded at Bangor. Observed water levels in Camden, 3 km north of Rockport, were 1 m higher than expected and 3.2 m larger than *PT* in Bangor. Estimations suggest that the flood reached its maximum water depth in Bangor over a period of just 15 minutes, which occurred 1 hour before high tide. Records of the storm in 1976 depict a very similar scenario to the October Windstorm. Anecdotally, local sources attributed the rapid onset of flooding in Bangor to an ice dam; however, the results of the present work suggest that perhaps high frequency tide-surge-river interaction contributed to the abruptly rising flood levels.

4.4 Comparison to Previous Research and Models

Tide-surge-river interaction resulting from the amplification of higher frequency harmonics is therefore an important part of *TS* in some estuaries but has been widely overlooked by extant research. In particular, previous work on tide-surge-river interaction in estuaries has generally neglected the contribution at the overtide frequencies, although some studies have acknowledged their existence in observations (Horsburgh & Wilson, 2007; Prandle & Wolf, 1978). Classic work on the topic utilized models that either linearize terms (analytically (Wolf, 1981; Proudman, 1955a, 1955b) and numerically (Horsburgh & Wilson, 2007; Rossiter, 1961;

433 Thomas et al., 2019; Prandle & Wolf, 1978)) and/or only allow nonlinear terms to be manifested
434 in surge as a phase shift of tide or surge relative to a non-stormy state. Consequently, the
435 observations associated with these studies focus on the mechanisms their models account for,
436 thus neglecting higher frequency nonlinearities. To the authors' knowledge, this is the first study
437 to identify and diagnose the development of 6th and 8th diurnal tide-surge-river interaction
438 generated by enhanced storm-induced currents and resonance. This work demonstrates that the
439 manner in which *LFS* manifests within an estuary can modify the magnitude of these currents
440 and oscillations, expanding upon the previous work outlining differences between externally and
441 internally generated storm surge (Horsburgh & Wilson, 2007). The previously neglected
442 nonlinear effects from overtide harmonics must be considered to accurately forecast surge in
443 inland systems.

444 Results from NOAA's Extratropical Storm Surge (ETSS) model during the October
445 Windstorm (Liu, 2019) reveal large discrepancies between observed and forecasted *TWL* when
446 nonlinear effects are significant (Fig. 8). Importantly, the ETSS model only includes tide and
447 *LFS* in determining *TWL*, and therefore does not capture increased water levels from river
448 discharge. By subtracting *PT* from *TWL* in Bangor immediately before the event, the
449 contribution to *TWL* from elevated river discharge was estimated to be about 0.35 m. With that
450 assumption, the model still underpredicts the *TWL* by 1.6 m in Bangor on day 30.4 (Fig. 8a),
451 showing that amplified higher frequency harmonics result in marked discrepancies between
452 observed and forecasted surges. Higher frequency tide-surge-river interaction is expected in
453 other systems that are shallow (< 15 m), quasi-prismatic, dominated by semi-diurnal tides and
454 are at lengths that are susceptible to resonance. Some examples include the upper Thames

455 estuary and Solent estuary on the British coast, where higher frequency storm surge has been
456 observed previously (Prandle & Wolf, 1978; Ozsoy et al., 2016).

457 **4.5 Effect of Climate Change**

458 The compounding effects of resonance are expected to be exacerbated by climate change.
459 Mean sea level (MSL) has been increasing globally at a rate near 1.7 mm yr^{-1} according to
460 estimations from coastal and island tide gauge measurements from 1900-2009, and near 3.4 mm
461 yr^{-1} according to satellite imagery estimates for 1993-2016 (Nerem et al., 2010; Church & White,
462 2011), with a net increase in MSL from 0.5 m to 1.2 m likely by 2100 (Kopp et al., 2014). These
463 rates are not constant world-wide, and climate models suggest that they will accelerate in coming
464 years (Nicholls & Casenave, 2010), making prediction capabilities even more difficult. In the
465 Penobscot River, considering the ideal depth for resonance of the D_8 is about 11 m and the mean
466 depth is near 8.5 m, any increase in MSL between those points will enhance the resonance
467 effects. Thus, sea level rise will effectively amplify higher frequency tide-surge-river interaction,
468 making storm surge flooding more frequent and more severe in some estuaries.

469 **4.6 Classic Harmonic Analysis Limitations**

470 It is important to note that the harmonic and wavelet analyses used in this study apply
471 strictly to linear systems, i.e. harmonics with constant amplitudes and phase. Riverine tides are
472 known for being strongly nonlinear from interactions between tidal constituents and fluctuating
473 freshwater discharge (e.g. Kukulka & Jay, 2003; Matte et al., 2013). By using the analysis
474 outlined in this paper, the tide and tidal species predicted are approximated and assumed to have
475 no nontidal influence from surge or river, making the tide-surge-river-interaction contain both
476 tide-surge and tide-river interactions. Using a non-stationary tidal analysis program like *NS_Tide*

(Matte et al., 2013), would allow for the separation of these terms from *I*, but there was insufficient data to accomplish this for the entire study period. That said, this analysis was deemed appropriate for the scope of this work, as the authors chose to focus on *net* nonlinear interactions through the tide-surge-river-interaction term. It is not possible to distinguish exactly how nonlinear tide-river interactions vary from tide-surge interaction using the analysis presented but is likely an important topic of future study.

5 Conclusions

Tide-surge-river interaction amplitudes were found to be more than double of low-frequency storm surge levels near the head of a macrotidal estuary. The D_6 and D_8 tidal frequency bands produced the largest contribution to the tide-surge-river interaction (~1 m). The enhancement of nonlinear quadratic friction from storm-induced currents was the main mechanism creating oscillations in the D_6, which were further amplified by resonance of the D_8 harmonic in the upper portion of the estuary. Tidally energetic estuaries near the resonant length of overtide harmonics (or a multiple of) are particularly at risk for high frequency tide-surge-river interaction events, which are expected to worsen in some systems with rising sea levels from climate change.

This research outlines the susceptibility of inland estuarine locations to extreme water level events, which we suspect will worsen in the future due to sea level rise and enhanced storminess. Currently, simple storm surge models do not include the nonlinear terms which explain high frequency tide-surge-river interaction, and so have the potential to under-predict total storm surges in estuaries. Other estuaries around the world may fit the criteria outlined in

this study, making them at risk of experiencing dangerous high frequency storm surge. Future research needs to include assessing the vulnerability of other systems and including tide-surge-river interaction in storm surge forecasting models, which will allow for public preparedness and better coastal planning to mitigate risk of inundation.

Acknowledgments

This project was funded by National Science Foundation Award IIA-1644691 and in part by National Science Foundation Award IIA-1355457. The authors offer sincere thanks to the citizen scientists who helped collect these data. This work would not have been possible without their efforts. The authors would also like to thank Kyah Lucky, Dylan Schlichting, Abby Roche, and Elliot Huguenard for help with sensor deployment, training citizen scientists, and transportation from the university. We also thank Stefan Talke and Pascal Matte for preliminary discussions on the data and path of the work, and two anonymous reviewers for their constructive comments on the manuscript. Data from this study are available online (http://dataverse.acg.maine.edu/dvn/faces/study/StudyPage.xhtml?globalId=hdl:TEST/10240&versionNumber=1.)

References

Álvarez Fanjul, E., Pérez Gómez, B., & Rodríguez Sánchez Arévalo, I. (2001). Nivmar: a storm surge forecasting system for Spanish waters. *Scientia Marina*, *65*(S1), 145-154. doi: 10.3989/scimar.2001.65s1145

Church, J., & White, N. (2011). Sea-Level Rise from the Late 19th to the Early 21st Century. *Surveys in Geophysics*, *32*(4-5), 585-602. doi: 10.1007/s10712-011-9119-1

Devlin, A., Jay, D., Talke, S., Zaron, E., Pan, J., & Lin, H. (2017). Coupling of sea level and tidal range changes, with implications for future water levels. *Scientific Reports*, *7*(1), 1-12. doi: 10.1038/s41598-017-17056-z

Dean, R. and Dalrymple, R. (1991). *Water Wave Mechanics for Engineers and Scientists*. Singapore: World Scientific Publishing Co. Pte. Ltd., pp.131-170.

Dudley, R.W. (2004). Estimating Monthly, Annual, and Low 7-Day, 10-Year Streamflows for Ungaged Rivers in Maine: U.S. Geological Survey Scientific Investigations Report 2004-5026, 22 p.

Feng, X., Olabarrieta, M., & Valle-Levinson, A. (2016). Storm-induced semidiurnal perturbations to surges on the US Eastern Seaboard. *Continental Shelf Research*, *114*, 54-71. doi: 10.1016/j.csr.2015.12.006

Friedrichs, C. (2010). Barotropic tides in channelized estuaries in *Contemporary Issues in Estuarine Physics* (ed. Valle-Levinson, A.), 27-61.

Geyer, W. (1993). Three-dimensional tidal flow around headlands. *Journal of Geophysical Research: Oceans*, *98*(C1), 955-966. doi: 10.1029/92jc02270

Geyer, W. (1997). Influence of Wind on Dynamics and Flushing of Shallow Estuaries. *Estuarine, Coastal and Shelf Science*, *44*(6), 713-722. doi: 10.1006/ecss.1996.0140

Geyer, W., & Ralston, D. (2018). A mobile pool of contaminated sediment in the Penobscot Estuary, Maine, USA. *Science of The Total Environment*, *612*, 694-707. doi: 10.1016/j.scitotenv.2017.07.195

Glahn, B., Taylor, A., Kurkowski, N. and Shaffer, W. (2009) The role of the SLOSH model in National Weather Service storm surge forecasting. *National Weather Digest*, 33(1), pp.3-14.

Hodgkins, G. A. (1999). Estimating the Magnitude of Peak Flows for Streams in Maine for Selected Recurrence Intervals: U.S. Geological Survey Water-Resources Investigations Report 99-4008, 45 p.

Holleman, R., & Stacey, M. (2014). Coupling of Sea Level Rise, Tidal Amplification, and Inundation. *Journal of Physical Oceanography*, *44*(5), 1439-1455. doi: 10.1175/jpo-d-13-0214.1

Horsburgh, K., & Wilson, C. (2007). Tide-surge interaction and its role in the distribution of surge residuals in the North Sea. *Journal of Geophysical Research*, *112*(C8), 1-13. doi: 10.1029/2006jc004033

Jones, J., & Davies, A. (2008). On the modification of tides in shallow water regions by wind effects. *Journal of Geophysical Research*, *113*(C5), 1-28. doi: 10.1029/2007jc004310

554 Kopp, R., Horton, R., Little, C., Mitrovica, J., Oppenheimer, M., & Rasmussen, D. et al. (2014).
555 Probabilistic 21st and 22nd century sea-level projections at a global network of tide-gauge
556 sites. *Earth's Future*, *2*(8), 383-406. doi: 10.1002/2014ef000239

557 Kukulka, T., & Jay, D. (2003). Impacts of Columbia River discharge on salmonid habitat: 1. A
558 nonstationary fluvial tide model. *Journal of Geophysical Research*, *108*(C9). doi:
559 10.1029/2002jc001382

560 Liu, H. (2019) Extratropical storm surge model data. NOAA, National Weather Service,
561 Meteorological Development Laboratory.

562 Lowe, J., & Gregory, J. (2005). The effects of climate change on storm surges around the United
563 Kingdom. *Philosophical Transactions of The Royal Society A: Mathematical, Physical and*
564 *Engineering Sciences*, *363*(1831), 1313-1328. doi: 10.1098/rsta.2005.1570

565 Lyddon, C., Brown, J., Leonardi, N., & Plater, A. (2018). Uncertainty in estuarine extreme water
566 level predictions due to surge-tide interaction. *PLOS ONE*, *13*(10), e0206200. doi:
567 10.1371/journal.pone.0206200

568 Matte, P., Jay, D., & Zaron, E. (2013). Adaptation of Classical Tidal Harmonic Analysis to
569 Nonstationary Tides, with Application to River Tides. *Journal of Atmospheric and Oceanic*
570 *Technology*, *30*(3), 569-589. doi: 10.1175/jtech-d-12-00016.1

571 Mercer, D. (2002). Barotropic waves generated by storms moving rapidly over shallow
572 water. *Journal of Geophysical Research*, *107*(C10), 1-17. doi: 10.1029/2001jc001140

573 Morrill, R., Chin, E. and Richardson, W. (1979) Maine Coastal Storm and Flood of February 2,
574 1976. *Geological Survey Professional Paper*, (1087), pp.1-17.

575 National Centers for Environmental Information. (2019). *Bathymetric Data Viewer*. [online]
576 Available at: https://maps.ngdc.noaa.gov/viewers/bathymetry/ [Accessed 4 Mar. 2019].

577 National Weather Service: Weather Prediction Center. (2017). *WPC's Surface Analysis Archive*.
578 [online] Available at: https://www.wpc.ncep.noaa.gov/archives/web_pages/sfc/sfc_archive.php
579 [Accessed 22 Mar. 2019].

580 Nayak, S., Bhaskaran, P., & Venkatesan, R. (2012). Near-shore wave induced setup along
581 Kalpakkam coast during an extreme cyclone event in the Bay of Bengal. *Ocean Engineering*, *55*,
582 52-61. doi: 10.1016/j.oceaneng.2012.07.036

583 Nerem, R., Chambers, D., Choe, C., & Mitchum, G. (2010). Estimating Mean Sea Level Change
584 from the TOPEX and Jason Altimeter Missions. *Marine Geodesy*, *33*, 435-446. doi:
585 10.1080/01490419.2010.491031

586 Nicholls, R., & Casenave, A. (2010). Sea-Level Rise and Its Impact on Coastal
587 Zones. *Science*, *328*(5985), 1517-1520. doi: 10.1126/science.1185782

588 Ozsoy, O., Haigh, I., Wadey, M., Nicholls, R., & Wells, N. (2016). High-frequency sea level
589 variations and implications for coastal flooding: A case study of the Solent, UK. *Continental*
590 *Shelf Research*, *122*, 1-13. doi: 10.1016/j.csr.2016.03.021

591 Parker, B. (1991). *Tidal Hydrodynamics* (pp. 237-419). New York: John Wiley & Sons, Inc.

Petterson, J., Stanley, L., Glazier, E., & Philipp, J. (2006). A Preliminary Assessment of Social and Economic Impacts Associated with Hurricane Katrina. *American Anthropologist*, *108*(4), 643-670. doi: 10.1525/aa.2006.108.4.643

Prandle, D., & Wolf, J. (1978). The interaction of surge and tide in the North Sea and River Thames. *Geophysical Journal International*, *55*(1), 203-216. doi: 10.1111/j.1365-246x.1978.tb04758.x

Pond, S. and Pickard, G. (1983). *Introductory Dynamical Oceanography*. 2nd ed. Burlington, MA: Elsevier Butterworth-Heinemann, pp.253-281.

Proudman, J. (1955a). The propagation of tide and surge in an estuary. *Proceedings of The Royal Society of London. Series A. Mathematical and Physical Sciences*, *231*(1184), 8-24. doi: 10.1098/rspa.1955.0153

Proudman, J. (1955b). The effect of friction on a progressive wave of tide and surge in an estuary. *Proceedings of The Royal Society of London. Series A. Mathematical and Physical Sciences*, *233*(1194), 407-418. doi: 10.1098/rspa.1955.0276

Qin, Z., Duan, Y., Wang, Y., Shen, Z., & Xu, K. (1994). Numerical simulation and prediction of storm surges and water levels in Shanghai harbour and its vicinity. *Natural Hazards*, *9*(1-2), 167-188. doi: 10.1007/bf00662597

Rego, J., & Li, C. (2010). Nonlinear terms in storm surge predictions: Effect of tide and shelf geometry with case study from Hurricane Rita. *Journal of Geophysical Research*, *115*(C6), 1-19. doi: 10.1029/2009jc005285

Rossiter, J. (1961). Interaction Between Tide and Surge in the Thames. *Geophysical Journal International*, *6*(1), 29-53. doi: 10.1111/j.1365-246x.1961.tb02960.x

Thomas, A., Dietrich, J., Asher, T., Bell, M., Blanton, B., & Copeland, J. et al. (2019). Influence of storm timing and forward speed on tides and storm surge during Hurricane Matthew. *Ocean Modelling*, *137*, 1-19. doi: 10.1016/j.ocemod.2019.03.004

Torrence, C., & Compo, G. (1998). A Practical Guide to Wavelet Analysis. *Bulletin of The American Meteorological Society*, *79*(1), 61-78. doi: 10.1175/1520-0477(1998)079<0061:apgtwa>2.0.co;2

Valle-Levinson, A., Olabarrieta, M., & Valle, A. (2013). Semidiurnal perturbations to the surge of Hurricane Sandy. *Geophysical Research Letters*, *40*(10), 2211-2217. doi: 10.1002/grl.50461

von Storch, H., & Woth, K. (2008). Storm surges: perspectives and options. *Sustainability Science*, *3*(1), 33-43. doi: 10.1007/s11625-008-0044-2

Wolf, J. (1978). Interaction of tide and surge in a semi-infinite uniform channel, with application to surge propagation down the east coast of Britain. *Applied Mathematical Modelling*, *2*(4), 245-253. doi: 10.1016/0307-904x(78)90017-3

Wolf, J. (1981) Surge-tide interaction in the North Sea and River Thames, in *Floods due to High Winds and Tides*, edited by Peregrine, D., pp. 75-94, Academic, London.

Zhang, J., Zheng, J., Jeng, D., & Guo, Y. (2015). Numerical Simulation of Solitary-Wave Propagation over a Steady Current. *Journal of Waterway, Port, Coastal, And Ocean Engineering*, *141*(3), 04014041. doi: 10.1061/(asce)ww.1943-5460.0000281

632 **Figures**

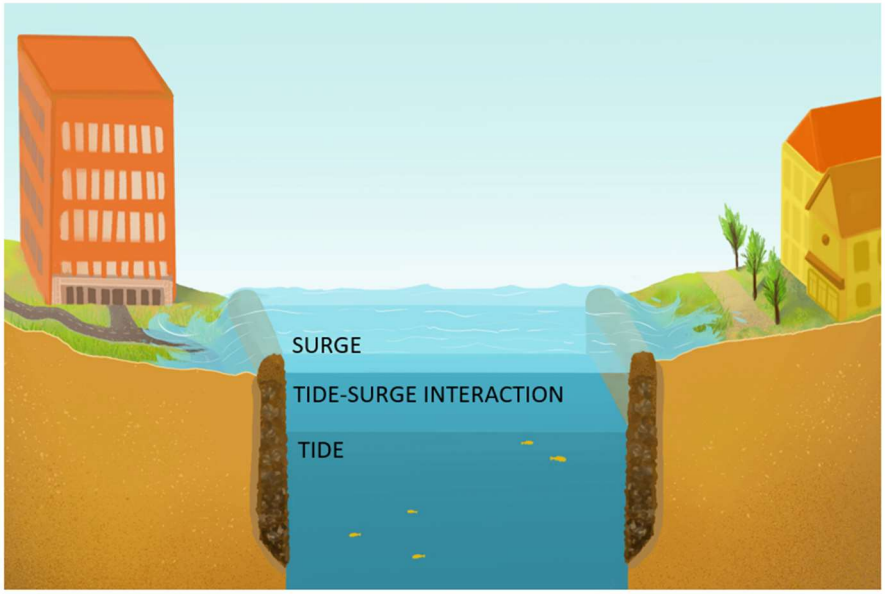

633

634 Figure 1: Conceptual view showing how tide-surge interaction and predicted storm surges can

635 create flooding scenarios in estuaries which would not occur without the interaction.

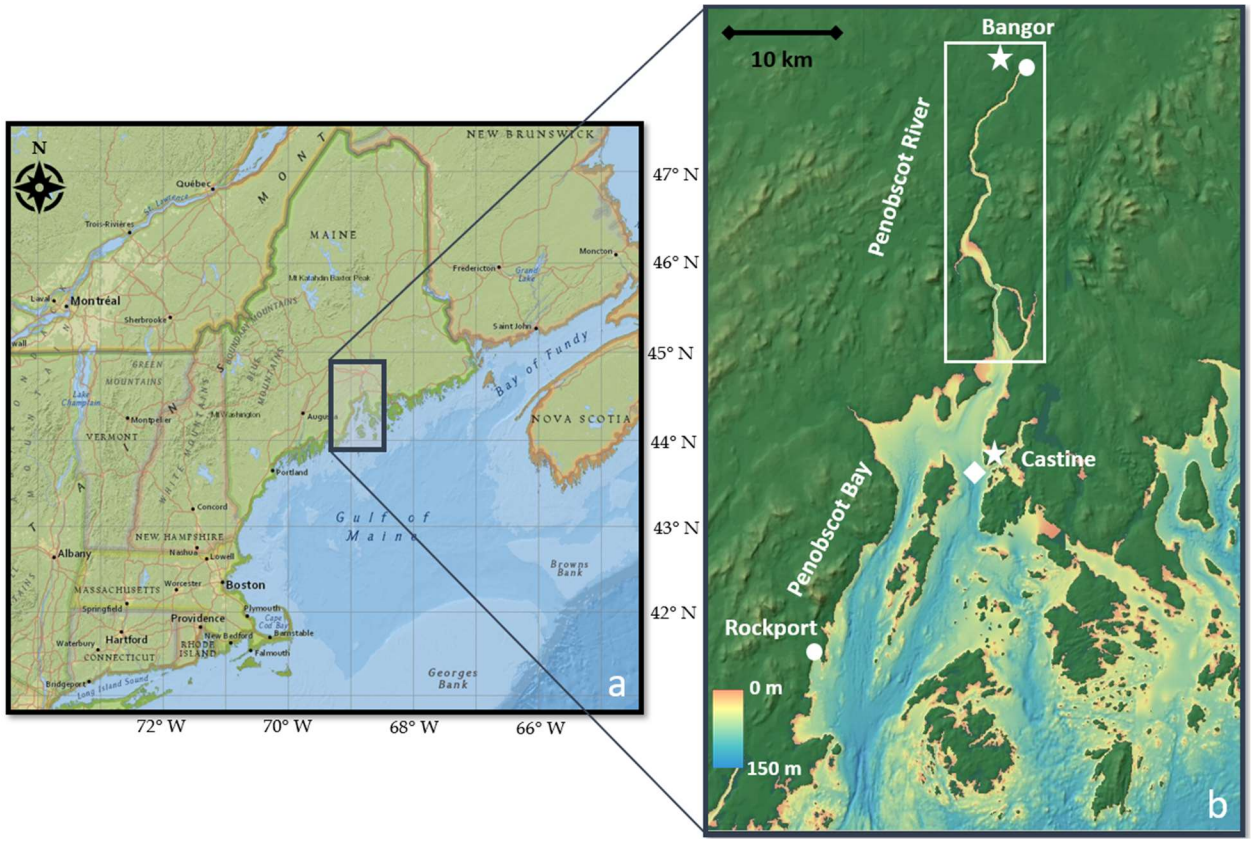

Figure 2: Study area in context of the coast of Maine and the Gulf of Maine [a] with data collection sites in the Penobscot Estuary [b] (National Centers for Environmental Information, 2019). Dots represent water level measurements, stars are barometric pressure and wind measurement locations, and the diamond is the measurement location of current velocities (water level measurements were also taken at Castine where the star is located).

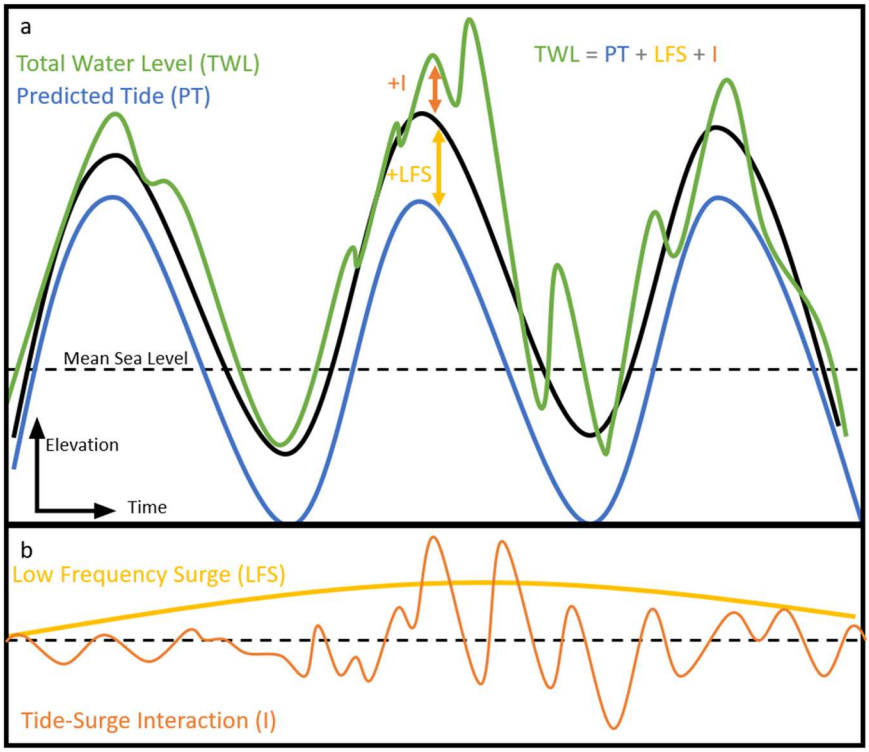

642

643 Figure 3: Conceptual diagram showing how low-frequency surge (*LFS*; yellow) and tide-surge-

644 river interaction (I; orange) [b] modify the predicted tide (*PT*; blue) to create the total water level

645 (*TWL*; green) [a]. The black line in [a] represents the total water level when tide-surge-river
646 interaction is negligible.

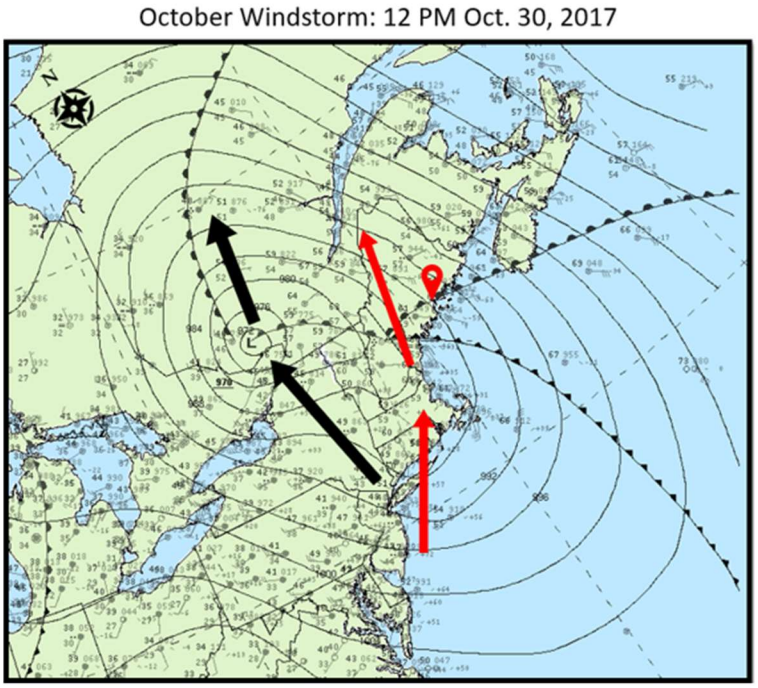

647

648 Figure 4: Storm tracks (arrows) and barometric pressure isobars for the October 17th, 2017
649 Windstorm (black) (National Weather Service: Weather Prediction Center, 2017) and February
650 1976 storm (red) (Morrill et al., 1979) relative to the Penobscot estuary, shown as the red marker.

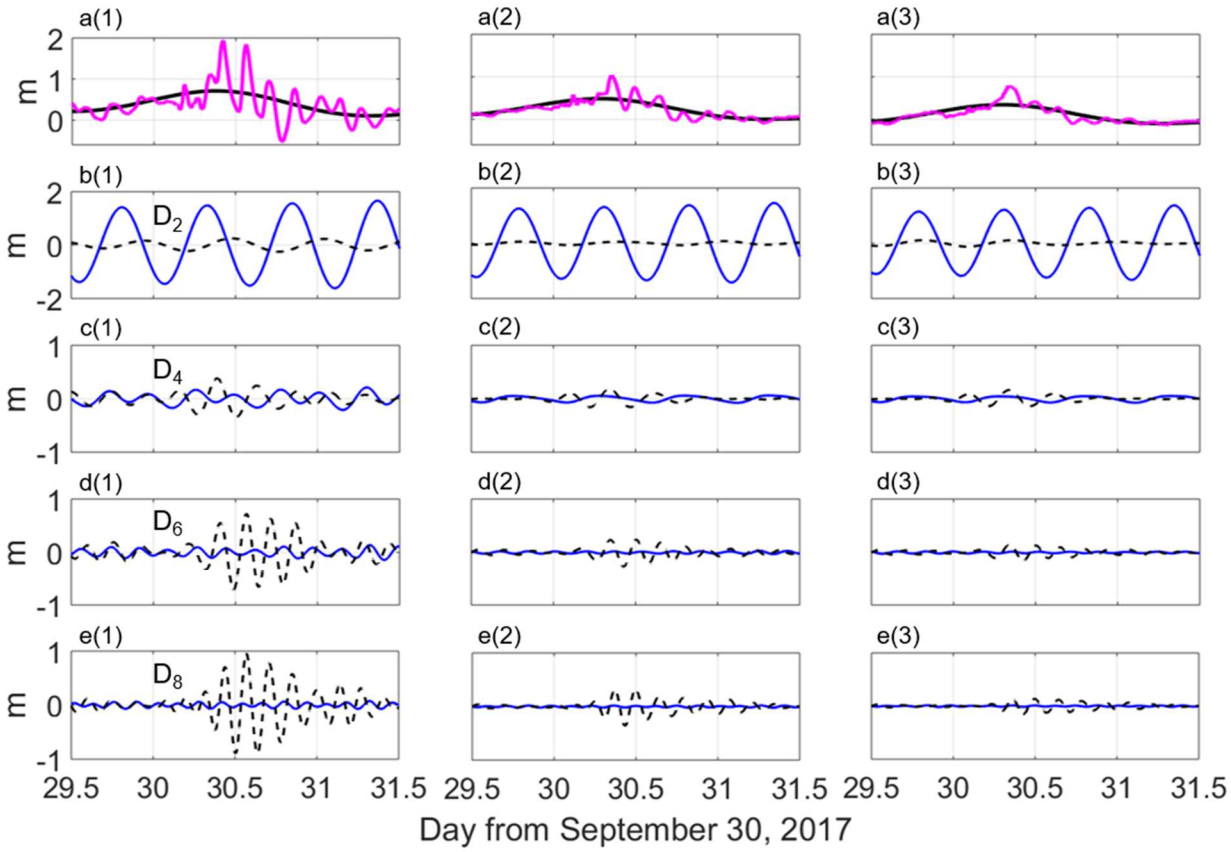

Figure 5: Low-frequency surge (*LFS*; solid black) and low frequency surge plus tide-surge-river interaction (*LFS+I*; magenta) [a]. Predicted tide (*PT*; blue) and tide-surge-river interaction (*I*;

654 dashed black) for the D_2 [b], D_4 [c], D_6 [d], and D_8 [e] bands at Bangor [1], Castine [2], and
655 Rockport [3] during the October Windstorm, beginning just prior to Day 30.

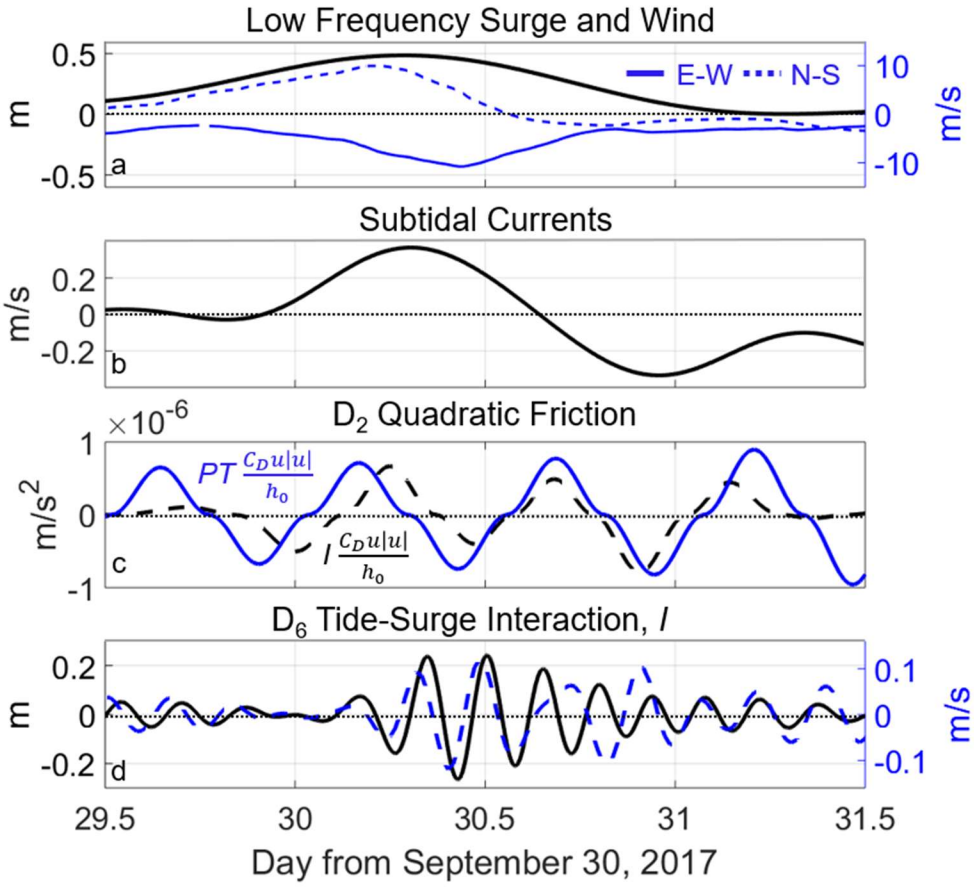

656

657 Figure 6: Low frequency surge (*LFS*; solid black), north-south component to wind (dashed blue),
658 and east-west component to wind (solid blue) during the October Windstorm [a], compared to
659 13-hour low pass filtered along channel (north south) current residuals [b], the D_2 quadratic
660 friction from predicted tide (solid blue) and tide-surge-river interaction (dashed black) [c], and

661 the D_6 tide-surge-river interaction in currents (dashed blue) and water level (solid black) [d]. All
662 measurement are from Castine except wind, measured in Bangor.

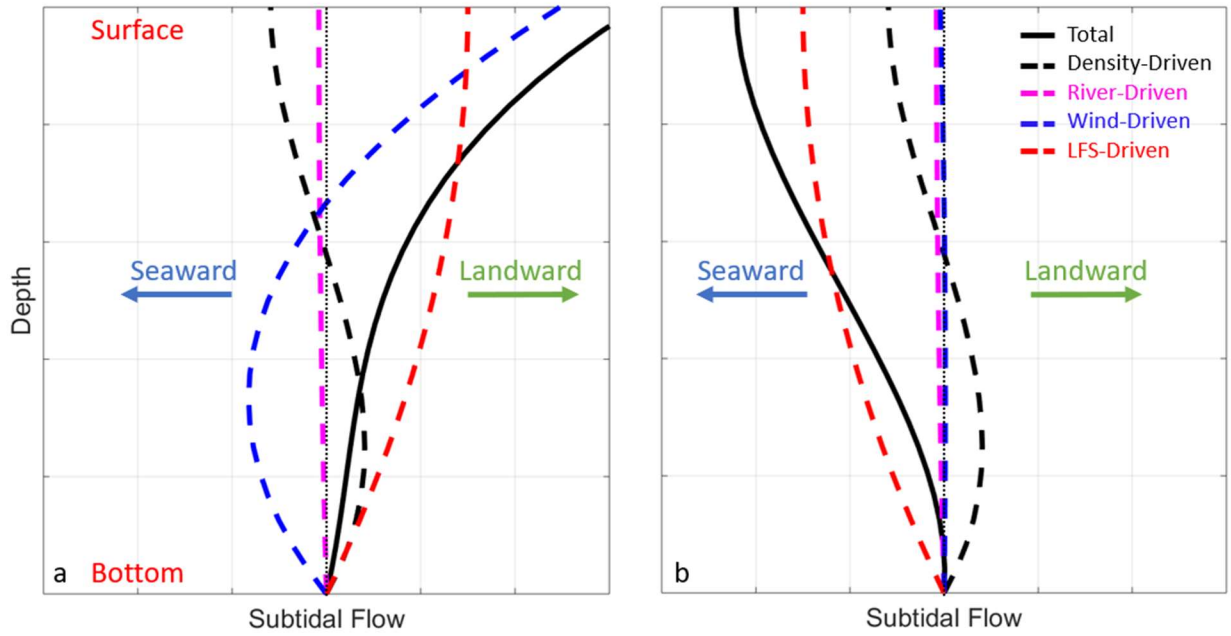

663

664 Figure 7: Conceptual figure of relative contributions to width-averaged, along channel non-tidal
665 flow from wind-induced (dashed blue), density-driven (dashed black), river (dashed magenta),
666 and *LFS* (dashed red) flows in Castine during the landward [a] and seaward [b] non-tidal flow
667 maxima during the October Windstorm. Total non-tidal flow is shown in solid black. Velocity

668 measurements taken at the Castine buoy were at a depth of 2 m – i.e., comparable to near-surface
669 flow

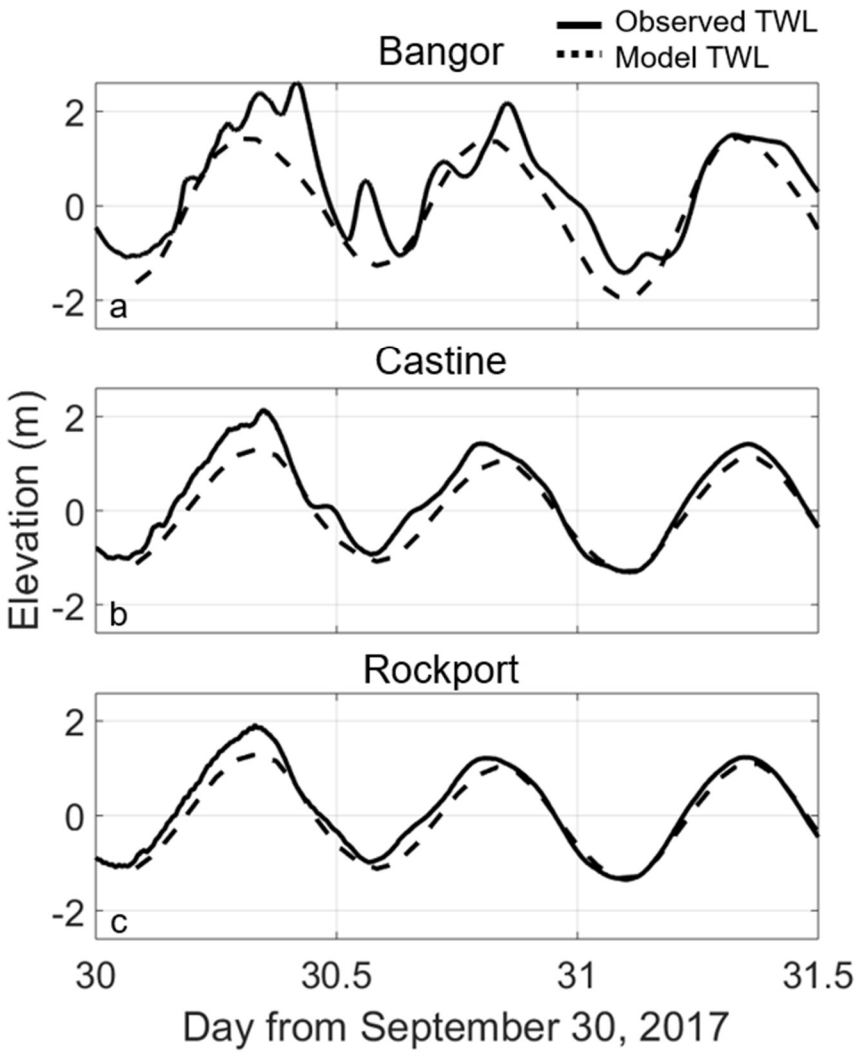

670

671 Figure 8: Observed total water level (*TWL*; solid) and NOAA Extra Tropical Storm Surge
672 (ETSS) tide plus surge forecasts (Liu, 2019) (dashed) in Bangor [a], Castine [b], and Rockport
673 [c] during the October Windstorm.

674